



OPEN ACCESS

EDITED BY

Ramin Rahmani,
Loughborough University,
United Kingdom

REVIEWED BY

Cetin Canpolat,
Çukurova University, Türkiye
Wei Zuo,
Wuhan University of Science and
Technology, China

*CORRESPONDENCE

Zhengquan Wu,
✉ wzqreal@163.com

RECEIVED 06 November 2025

REVISED 11 February 2026

ACCEPTED 11 February 2026

PUBLISHED 02 March 2026

CITATION

Wu Z and Zhuo G-h (2026) Considering
surface roughness O-ring lubricating-oil
static seal leakage prediction via
optimized circular plate gap model.
Front. Mech. Eng. 12:1740843.
doi: 10.3389/fmech.2026.1740843

COPYRIGHT

© 2026 Wu and Zhuo. This is an open-
access article distributed under the terms
of the [Creative Commons Attribution
License \(CC BY\)](#). The use, distribution or
reproduction in other forums is permitted,
provided the original author(s) and the
copyright owner(s) are credited and that
the original publication in this journal is
cited, in accordance with accepted
academic practice. No use, distribution or
reproduction is permitted which does not
comply with these terms.

Considering surface roughness O-ring lubricating-oil static seal leakage prediction via optimized circular plate gap model

Zhengquan Wu^{1,2*} and Guo-hai Zhuo³

¹School of Mechanical Engineering, Henan Institute of Technology, Xinxiang, China, ²Henan Provincial Engineering Technology Research Center for Digital Design and Manufacturing of Electromechanical Equipment, Xinxiang, China, ³Shanghai Microelectronics Equipment (Group) Co., Ltd., Shanghai, China

Introduction: O-ring seals are critical to ensuring the reliability of mechanical systems under harsh operating conditions. However, the classical parallel plate leakage model often neglects the effects of surface roughness and radial pressure distribution, leading to insufficient prediction accuracy. This study addresses this limitation by extending the classical parallel plate leakage theory to develop an optimized circular plate gap leakage model for O-rings.

Methods: A leakage rate correction factor μ 1 is introduced to quantify the effect of surface roughness, establishing an equivalent relationship between the micro-scale rough interface and the ideal smooth surface. The leakage rates of rough surfaces with different roughness levels under various differential pressures are theoretically calculated. Experimental validation is carried out under differential pressures of 0.3 MPa and 0.6 MPa, as well as surface roughness Ra values of 0.8 μm , 1.6 μm , and 3.2 μm .

Results: At a differential pressure of 0.4 MPa, the leakage rate reaches $0.67 \times 10^{-12} \text{ m}^3/\text{s}$ when $Ra = 3.2\mu\text{m}$, which is 1.8 times that of the case with $Ra = 0.8\mu\text{m}$. Experimental results show that: (1) At the same surface roughness, the cumulative leakage volume increases with the increase of differential pressure; when $Ra = 1.6\mu\text{m}$, the cumulative leakage volume at 0.6 MPa is approximately 1.5 times that at 0.3 MPa. (2) At the same differential pressure, a larger Ra results in a higher cumulative leakage volume; at 0.3 MPa, the cumulative leakage volume at $Ra = 3.2\mu\text{m}$ is about 1.7 times that at $Ra = 0.8\mu\text{m}$. Overall, the leakage rate increases almost linearly with the increase of both differential pressure and surface roughness. The relative error between theoretical and experimental values is within 15%.

Discussion: The relative error within 15% confirms the reliability of the proposed model. However, uncertainties in the model primarily stem from unaccounted factors, including high temperature, long-term O-ring aging, extreme high pressure, and idealized model assumptions. Consequently, the model is only valid under conditions of room temperature, low pressure, and short-term service. Nevertheless, this work provides a robust analytical framework for O-ring leakage prediction and sealing performance optimization in engineering applications.

KEYWORDS

circular plate gap leakage model, finite element simulation, leakage rate, O-ring seal, surface roughness

1 Introduction

O-ring seals are indispensable components in modern mechanical systems, renowned for their structural simplicity, cost-effectiveness, and superior self-sealing capability. They play an irreplaceable role in ensuring operational reliability and are widely used in fields such as aerospace, hydraulic engineering, deep-sea exploration, and precision machinery (Yu et al., 2025; Vijayaragavan et al., 2025; Yang et al., 2023). The sealing mechanism of O-rings relies on two core stages: during initial installation, compression between the sealing surface and groove base generates pre-tightening forces to achieve preliminary sealing; in operational conditions, fluid pressure applied to one side induces lateral deformation (reshaping the seal into a characteristic D-profile), thereby amplifying the interfacial contact pressure. Effective leakage prevention is only achieved when this contact pressure exceeds the external fluid pressure, transitioning the sealing system into a stable state that suppresses fluid or gas permeation.

With the deepening of sealing research, researchers must consider not only the influence of contact pressure but also the impact of surface roughness texture on leakage. Currently, static seal leakage calculation models primarily fall into two categories: one equates the rough interface of the seal to a porous medium for leakage calculation (Huon et al., 2021), and the other evaluates leakage through channels formed by liquid flow in the sealing gaps of rough surfaces (Tong et al., 2024). Zhao et al. (2022) utilized a white-light interferometer to measure surface roughness distribution, established a three-dimensional percolation grid model, and explored the effects of rough surfaces and material properties on porosity and leakage rate. Wu et al. (2024) treated pits and scratches as “pores” within porous media based on finite element analysis of their significantly enlarged equivalent gaps, calculating leakage via gap distribution. Kerr and Nielson (2022) integrated molecular dynamics simulation with *in-situ* monitoring technology to construct a multi-physical-field multi-scale coupling model.

The flat-plate gap leakage model, pioneered by Persson (2022), serves as the theoretical cornerstone for O-ring leakage prediction. Operating under the parallel-plate assumption, this model describes leakage through the Poiseuille flow equation and has been widely applied in engineering design. However, in real-world working conditions, factors such as the nonlinear deformation of rubber, medium penetration, and surface topography (Wu et al., 2024) significantly reduce the model's predictive accuracy. Even for conventional hydraulic media, the dynamic coupling between fluid pressure and rubber deformation dynamically modulates the sealing gap: higher pressure enhances the self-tightening effect, but excessive pressure may cause irreversible deformation of O-rings, leading to sealing failure (Zhao et al., 2025).

The hyperelastic and viscoelastic properties of rubber substantially alter gap distribution: Song et al. (2024) adopted the Mooney-Rivlin constitutive model and found that increasing the O-ring compression rate from 15% to 25% expanded the contact width by 58% and reduced the average gap by 42%. Surface roughness and defects of the sealing interface are also key factors affecting leakage: Zhao et al. (2022) measured via white-light interferometry that at a surface roughness $Ra = 0.8 \mu\text{m}$, the actual contact area was 27% higher than the theoretical value, with the equivalent gap reduced by 22%. For metal O-rings, Qi et al. (2023) found that an open-hole structure (hole diameter $\varphi 2 \text{ mm}$, hole spacing $2D$) reduced the stress concentration

coefficient by 40% and controlled gap fluctuation within $\pm 10\%$. Wang et al. (2023) defined leakage channels as two typical forms by uniformly arranging the triangular peaks of rough surface profiles, and proposed a leakage rate calculation method based on a composite channel model grounded in the leakage theory of gaps between parallel fixed flat plates.

In practical working conditions, pressure-medium coupling effects significantly alter leakage characteristics: Mo et al. (2025) studied CO_2 medium and found that rapid decompression (from 50 MPa to 0 MPa in 1 s) induced microcracks in rubber, increasing the equivalent gap by three orders of magnitude, and thus proposed a crack propagation correction factor. Zhang and Xie (2018) classified rough bodies into elastic, elastoplastic, and plastic regions based on characteristic lengths, conducted mathematical modeling of leakage channels under contact surfaces using fractal theory, and established fractal models for both the contact and leakage processes to investigate fluid leakage through metal sealing surfaces.

Despite the development of advanced models, they either involve complex computations or oversimplify interface characteristics. To address these limitations, this study proposes an optimized circular-plate gap leakage model tailored for O-rings through theoretical derivation of the classical parallel-plate framework. The key innovations are twofold: first, integrating radial pressure continuity and flow rate conservation constraints to adapt to the annular geometry of O-rings, resolving the deficiency of the uniform pressure assumption; second, introducing a novel leakage rate correction factor by establishing equivalence relationships between microscale rough interfaces and idealized smooth surfaces, explicitly quantifying the influence of surface roughness on leakage channels. Subsequent numerical simulations systematically quantify the contact lengths and pressure distributions under varying compressive loads.

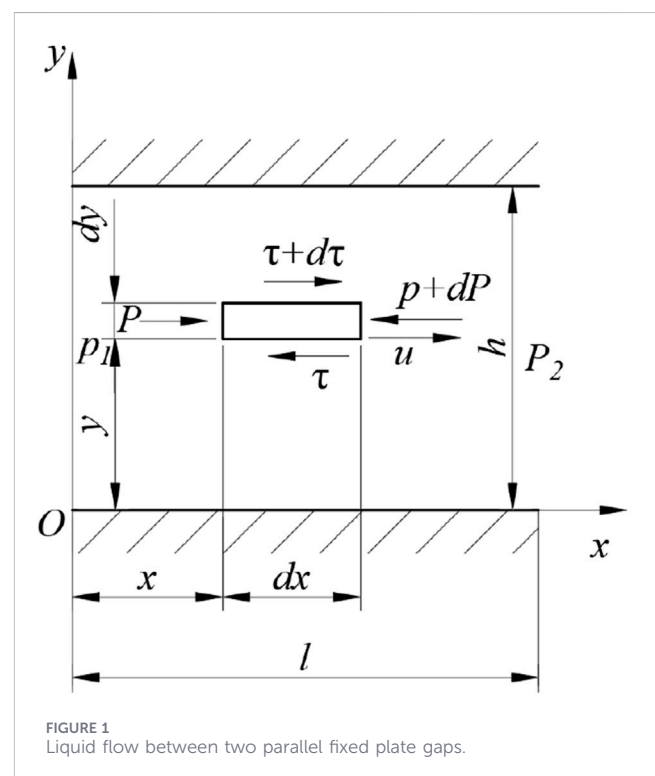


FIGURE 1
Liquid flow between two parallel fixed plate gaps.

The proposed model demonstrates high-fidelity predictive capabilities across diverse sealing pressures and surface roughness profiles, providing a robust analytical framework for optimizing O-ring performance in engineering scenarios requiring stringent leakage control.

2 Model of circular plate gap leakage

Between the gaps of two parallel plates is filled with liquid. The gap height is h , the length of the plate channel is l , and the width is b . The liquid within the parallel plate gaps is influenced by both the pressure difference and the relative motion of the plates. In the liquid flow, a micro-element $dx dy$ is taken. The pressures acting on its left and right end faces are p and $p + dp$, while the shear stresses on the upper and lower surfaces are τ and $\tau + d\tau$. The force condition is illustrated in Figure 1.

From the force balance equation, we can derive (Equation 1):

$$pb dy + (\tau + d\tau)b dx = (p + dp)b dy + \tau b dx \tag{1}$$

Then, according to the friction law of viscous fluid $\tau = -\eta \partial u / \partial y$, through integration, the formula for calculating the flow velocity of the liquid flowing through the parallel plate gap with width b is:

$$u = -\frac{\Delta p y^2}{2\eta l} + C_1 y + C_2 \tag{2}$$

In the formula: Δp is the pressure difference at both ends of the gap, $\Delta p = p_1 - p_2$; η is the dynamic viscosity of the fluid (Pa·s). The leakage of the liquid flowing through the gap between two parallel plates is caused by the pressure difference. Substitute the boundary conditions (when $y = 0, u = 0$; $y = h, u = 0$) into Equation 2 respectively to solve for the constants C_1 and C_2 . Through integration, the calculation formula the leakage channel can be obtained, as shown in Equation 3:

$$Q = \int_0^h u b dy = \frac{bh^3 \Delta p}{12\eta l} \tag{3}$$

To achieve accurate calculation of the O-ring leakage rate Q , an annular flat-plate clearance leakage model was established. The core logic of this model is as follows: after the O-ring undergoes compressive deformation, the leakage coupling effect between annular micro-elements is essentially governed by two key physical constraints—continuous radial pressure distribution and global conservation of incompressible fluid flow rate. Specifically, the outlet pressure of the previous micro-element equals the inlet pressure of the subsequent micro-element, and the total leakage rate remains constant throughout the entire flow channel.

The core constraint conditions of the model are detailed as follows.

2.1 Pressure continuity constraint

Fluid flows from the high-pressure side at the inner diameter to the low-pressure side at the outer diameter of the O-ring seal, with pressure showing a continuous gradient attenuation along the radial direction. For any two adjacent radially discrete micro-elements i

and $i + 1$, the condition “outlet pressure of micro-element $i =$ inlet pressure of micro-element $i + 1$ ” is satisfied, thereby forming an uninterrupted radial pressure distribution field.

2.2 Flow rate conservation constraint

Based on the incompressible fluid assumption, the total leakage rate Q passing through the sealing clearance is globally constant. For any single micro-element divided along the radial direction, its local leakage rate dQ_i is equal to the total leakage rate Q , i.e., $dQ_i = Q$.

The solution procedure of the model follows the approach of micro-element discretization → coupling relationship establishment → integration and combination of total pressure difference, which transforms the complex micro-element coupling problem into a single-variable solution problem targeting the total leakage rate Q . The specific steps are as follows:

Step 1: Maintain the discretization of annular micro-elements.

Divide N equally wide micro-elements along the radial direction of the sealing contact (from r_1 to r_2 , where $(N \geq 20)$ to ensure the pressure gradient is approximately linear. The key parameters of the micro-elements are defined as follows.

- Micro-element width: $dr = (r_2 - r_1) / N$;
- Central radius of the micro-element: $r_i = r_1 + (i - 0.5) dr$;
- Micro-element circumference (serving as the leakage channel width): $2\pi r_i$;
- Micro-element leakage path length (radial flow distance): dr .

Step 2: Establish the coupling relationship between annular micro-elements.

Based on the flow rate conservation constraint ($dQ_i = Q$) and the viscous flow formula, the coupling relationship between the pressure difference across each micro-element and the total leakage rate Q is derived as follows.

2.3 Leakage rate formula for a single micro-element (considering coupling)

For the i -th micro-element, the fluid flow obeys the Hagen-Poiseuille law (viscous laminar flow), and its local leakage rate is expressed as:

$$dQ_i = \frac{\mu_1(r_i) \cdot 2\pi r_i \cdot h(r_i)^3 \cdot d\Delta p_i}{12\mu dr} \tag{4}$$

Based on the flow rate conservation constraint ($dQ_i = Q$), the pressure difference across the i -th micro-element can be rearranged to obtain:

$$d\Delta p_i = \frac{Q \cdot 12\mu \cdot dr}{\mu_1(r_i) \cdot 2\pi r_i \cdot h(r_i)^3} \tag{5}$$

In the formula: μ_1 —Leakage rate correction factor, a coefficient accounting for the blockage/contraction effects of surface roughness on leakage channels; μ —Dynamic viscosity of the fluid. The stronger the viscous resistance of fluid flow, the smaller the leakage rate.

$\mu_1(r_i)$ and $h(r_i)$ denote the correction factor and sealing clearance of the i -th micro-element, respectively. Owing to the arched distribution of contact pressure $p(r)$, both parameters vary with r_i .

2.4 Coupled integral equation for total pressure difference

The total pressure difference Δp (i.e., high pressure at the inner diameter minus low pressure at the outer diameter) equals the sum of the pressure differences across all micro-elements, which arises from the continuous radial superposition of pressure:

$$\Delta p = \sum_{i=1}^N d\Delta p_i = \int_{r_1}^{r_2} \frac{Q \cdot 12\mu \cdot dr}{\mu_1(r) \cdot 2\pi r \cdot h(r)^3} \quad (6)$$

In the formula: r_1 is the inner diameter of the ring at the sealing contact; r_2 is the outer diameter of the ring at the sealing contact.

By rearranging and combining (Equations 4–6), the coupled solution formula for the total leakage rate Q is obtained as Equation 7.

$$Q = \frac{\Delta P \cdot 2\pi}{12 \cdot \mu} \cdot \frac{1}{\int_{r_1}^{r_2} \frac{dr}{\mu_1(r) \cdot r \cdot h(r)^3}} \quad (7)$$

Step 3: Substitute Coupling Parameters (Address the Radial Variation of $h(r)$ and $\mu_1(r)$)

The coupling between micro-elements is also reflected in the radial variation of $h(r)$ and $\mu_1(r)$ with the radial position r (owing to the arched distribution of contact pressure $p(r)$), which requires accurate calculation according to the following method.

2.5 Leakage rate correction factor $\mu_1(r)$ (considering roughness coupling)

Yang (2016) used 39 different geometric models to analyze the influence of surface roughness and gap height on the leakage rate, and fitted the expression of the leakage rate correction factor μ_1 :

$$\mu_1(r) = 1 - \exp \left[-0.6 \left(\frac{h(r)}{T} \right)^{0.33} \left(\frac{\delta}{T} \right)^{-0.96} \right] \quad (8)$$

In the formula: δ is the root mean square deviation of the surface profile; T is the surface autocorrelation length, reflecting the density of peaks on the actual engineering surface (Yang, 2016). Engineering value range of T : Precision-ground surface: $T = 0.5\text{--}1.0 \mu\text{m}$; Conventional turned surface: $T = 1.0\text{--}2.0 \mu\text{m}$; Rough-machined surface: $T = 2.0\text{--}3.0 \mu\text{m}$. As T increases, the peak-valley structures on the surface become sparser, and the rate of change of μ_1 with respect to δ/T slows down.

2.6 Sealing clearance $h(r)$ (considering contact pressure coupling)

The surface roughness of the O-ring is determined by the morphology of the mold surface during its vulcanization. For metal surface profiles processed by precision turning, precision grinding, and lapping, the ratio of the root mean square deviation δ to the arithmetic mean deviation Ra of the profile is 1.22~1.27. In this study, the intermediate value is adopted (Yasuo et al., 2017), namely:

$$\delta = 1.25Ra \quad (9)$$

When considering the influence of roughness on the leakage channel for the leakage rate of the annular flat - plate sealing model, when the sealing surface of rubber seal is not subjected to pressure, the initial contact height is taken as $h_0 = 3\delta$; when the pressure is Δp , the sealing gap is h , and its calculation formula is as follows (Roth, 1972):

$$h(r) = h_0 e^{-\frac{\Delta p}{\lambda}} = 3\delta e^{-\frac{\Delta p}{\lambda}} \quad (10)$$

where λ is the sealing coefficient of the O-type rubber seal material.

Since the roughness value of the metal contact surface is far smaller than that of the rubber surface, the real contact state between the O-ring and the rough interface can be regarded as the contact between an elastic rough surface and a rigid smooth surface. Therefore, the rough peaks on the contact surface of the O-ring are simplified into a cone with a cone angle of 120° and a height of h_0 . An axisymmetric plane model is adopted, as shown in Figure 2. The upper cylinder is a metal rigid body, and the lower cone is a rubber deformable body. The rubber material uses silicone rubber consistent with the O-ring material, with a Shore hardness of 50 HA. It is assumed that the mechanical properties of the rubber material are incompressible, so the Mooney-Rivlin model is adopted.

The relationship between the sealing coefficient λ and medium pressure p depends on the hyperelastic sealing behavior of the O-ring, material properties, and surface contact conditions. As a hyperelastic material, the contact stress of the O-ring exhibits a nonlinear increase with p ; the higher the pressure, the tighter the O-ring is compressed, resulting in a higher contact stress.

For silicone rubber with Shore Hardness 50 HA, which features low hardness and high elasticity, the deformation saturation effect is more pronounced. Its relationship with p can be expressed in the form of exponential decay:

$$\lambda = \lambda_0 \cdot e^{-\alpha p} + \lambda_\infty \quad (11)$$

In the formula: λ_0 - Initial sealing coefficient, with $\lambda_0 = 2.8$ as $p \rightarrow 0$; α - Exponential decay coefficient, taken as $\alpha = 0.52 \text{ MPa}^{-1}$; λ_∞ - Sealing coefficient at pressure saturation, with $\lambda_\infty = 0.35$ as $p \rightarrow \infty$. or typical operating conditions with $p = 0.3 \text{ MPa}$ and $p = 0.6 \text{ MPa}$, the corresponding sealing coefficients are 2.747 and 2.399, respectively.

Step 4: Numerically Solve the Total Leakage Rate Q .

Since $h(r)$ and $\mu_1(r)$ vary nonlinearly with r , Equation 7 has no analytical solution and is thus solved using the trapezoidal numerical integration method.

2.7 Discrete calculation of the integral term $f(r_i)$

When the radial sealing range of the O-ring (from r_1 to r_2) is divided into N annular micro-elements, $N+1$ micro-element endpoints are obtained (from the start point of the first micro-element to the end point of the last micro-element), denoted as $r_0, r_1, r_2, \dots, r_N$. For the central radius r_i of each micro-element, the integral term is calculated as follows:

$$f(r_i) = \frac{1}{\mu_1(r_i) \cdot r_i \cdot h(r_i)^3} \quad (12)$$

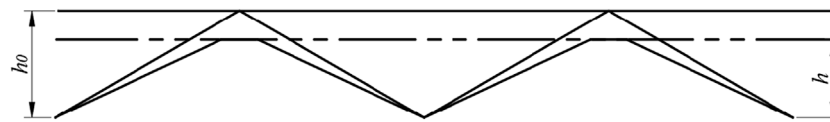


FIGURE 2
Schematic diagram of rough surface contact height.

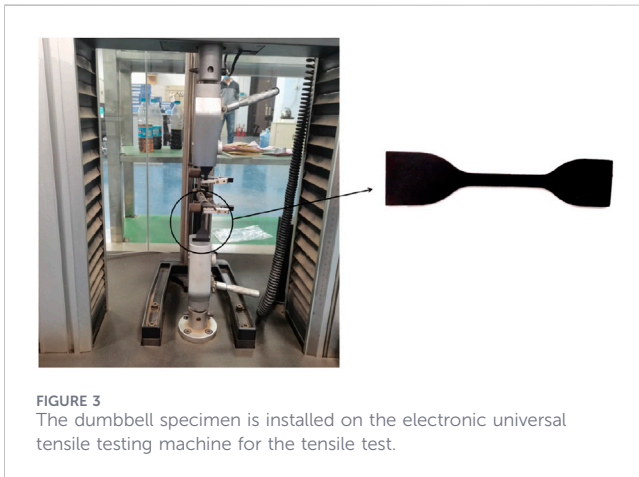


FIGURE 3
The dumbbell specimen is installed on the electronic universal tensile testing machine for the tensile test.

2.8 Calculation of integral value I via trapezoidal method

$$I = \int_{r_1}^{r_2} f(r)dr \approx \frac{dr}{2} \left[f(r_0) + 2 \sum_{i=1}^{N-1} f(r_i) + f(r_N) \right] \quad (13)$$

Herein, r_0 denotes the start point of the integral interval, which corresponds to the inner diameter r_1 of the O-ring sealing contact; r_N denotes the end point of the integral interval, corresponding to the outer diameter r_2 of the O-ring sealing contact.

Parameters including pressure $p(r)$, r_1 , r_2 , and $h(r)$ need to be obtained via finite element simulation of the O-ring compressed by the medium pressure in the groove, which yields the radial contact length and pressure distribution on the sealing contact surface. By substituting the relevant parameters derived from Equations 8–13 into Equation 7, the total leakage rate Q can be calculated.

3 Experiments and numerical implementation

3.1 Determination of material constitutive model parameters

Rubber specimens are made into Type I dumbbell-shaped specimens in accordance with the national standard GB/T 528–2009. The specimen thickness is (2 ± 0.2) mm, and the length of the test section is (25 ± 0.5) mm. Three dumbbell specimens are prepared from the same rubber compound, and the experimental results are averaged. The experimental

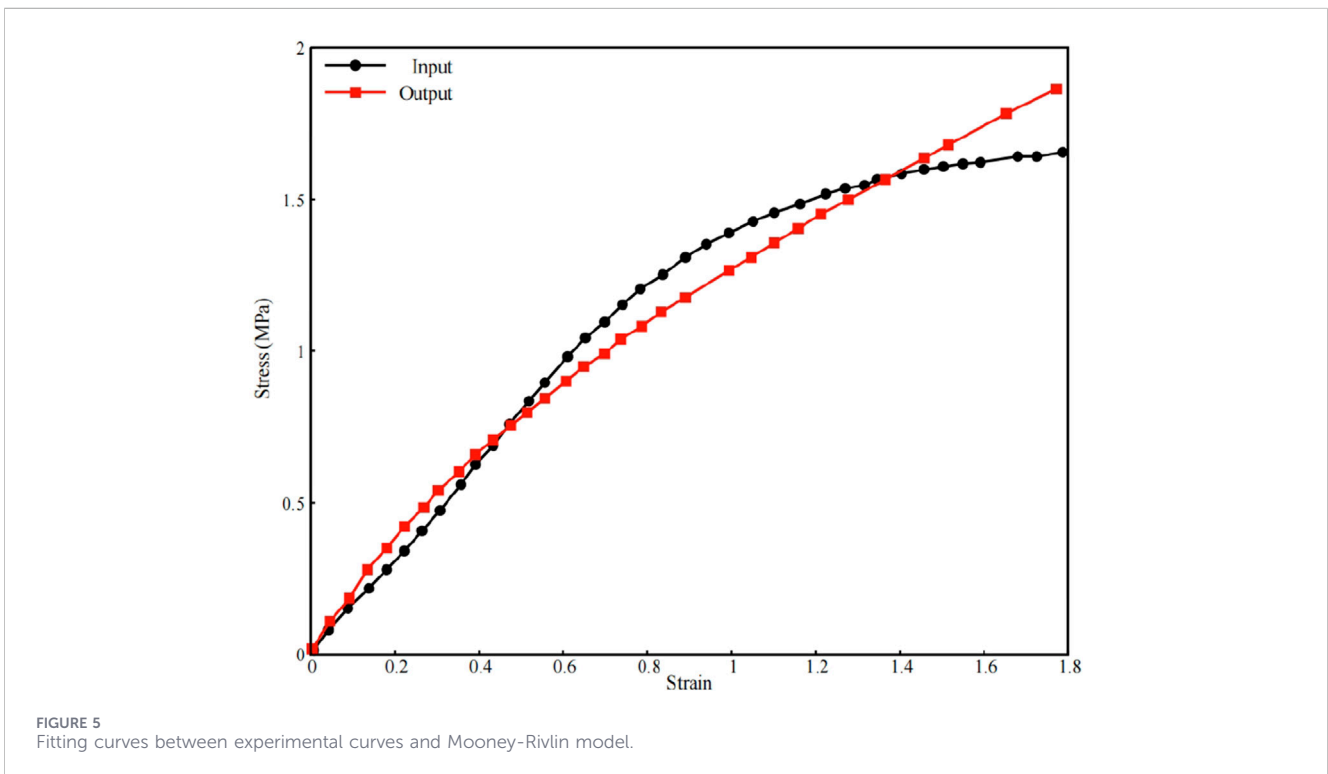
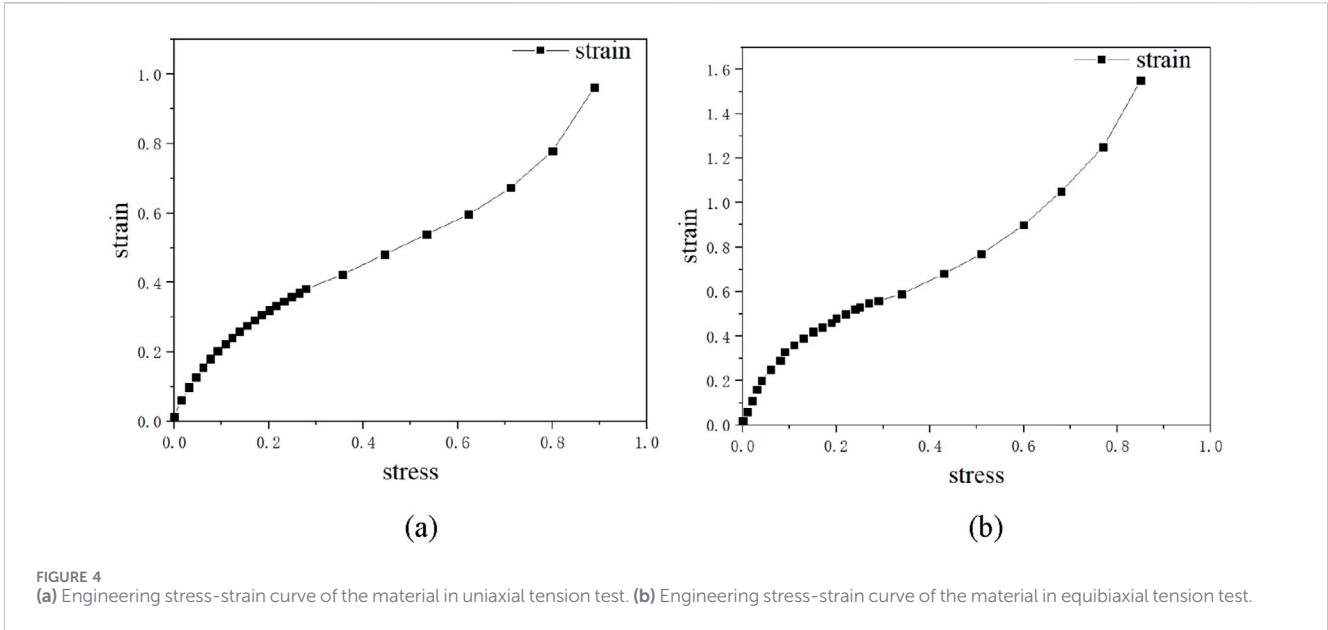
equipment is a WDW-20 Micro-controlled Electronic universal testing machine, as shown in Figure 3. The prepared dumbbell specimens are installed on the electronic universal tensile testing machine, and stretching begins at a constant rate of (500 ± 50) mm/min until the specimen fails, recording the load-displacement curve.

As illustrated in Figure 4a, the experimentally recorded load-displacement curve is normalized into an engineering stress-strain profile, where tensile stress (ordinate) and tensile strain (abscissa) characterize the material's mechanical response. The derived curve exhibits pronounced nonlinear hyperelastic behavior, a hallmark of rubber materials. Notably, at a strain level of 0.8, the material demonstrates significant strain accommodation with minimal stress increment, indicative of its molecular chain reorientation under load. To further quantify multiaxial deformation characteristics, equibiaxial tensile testing was conducted using an ERBI-300 inflatable testing system, compliant with the GB/T 528–2009 international standard for tensile property evaluation of vulcanized and thermoplastic rubbers. The resulting equibiaxial strain-stress relationship, shown in Figure 4b, reveals distinct anisotropic stiffening behavior compared to uniaxial loading conditions.

For the rubber material of the O-ring seal, reliable stress-strain curves are derived through experimental data from uniaxial tension, equibiaxial, and planar shear tests, based on appropriate constitutive models like Mooney-Rivlin, Yeoh, Ogden, etc. The most widely used is the Mooney-Rivlin model, capable of simulating the mechanical properties of most rubber materials. This model typically includes four equation types with 2, 3, 5, or 9 parameters—more parameters yielding higher fitting accuracy. The compression ratio of the O-ring adopted in this study falls within the moderate deformation range, and the strain energy density function of the two-parameter Mooney-Rivlin model, expressed as $W=C_{10}(I_1-3) + C_{01}(I_2-3)$, can accurately characterize the hyperelastic behavior of the O-ring within this deformation interval.

This study selects the 2-parameter Mooney-Rivlin model, widely applied in laboratories for rubber material analysis. The rubber's stress-strain curve shows nonlinearity, with its mechanical behavior closely linked to factors such as experimental environment, working conditions, and loading rate. According to the uniaxial tension engineering stress-strain data measured by the electronic universal tensile testing machine and the equibiaxial tension engineering stress-strain curve, the 2-parameter Mooney-Rivlin model is used. As shown in Figure 5, fitting the experimental curve with the Mooney-Rivlin model yields two parameters: $C_{10} = 0.27$, $C_{01} = 0.03$.

For the simulation model, one end is fixed, and the other end uses the RBE element to grasp partial nodes for applying a forced displacement of 50 mm. The reaction force of RBE nodes is extracted and compared with the experimental tension under the same tensile



displacement. As shown in Figure 6, the numerical values of the two are highly close, thereby verifying the correctness of the constitutive model.

As shown in Figure 7, when one end of the specimen is stretched by 50 mm, the equivalent stress of the specimen reaches a maximum of 10.92 MP, and the width of the narrow part changes from 6 mm to 4.4 mm. The maximum tensile stress during the specimen’s stretching-to-fracture process is the tensile strength. Experiments show that the specimen’s tensile strength is approximately 18.5 MP.

3.2 Numerical implement of O-ring sealing

Taking a certain sealing device as an example, the dimensions of the O-ring and the groove structure are shown in Figure 8. The sealing medium of this sealing device is hydraulic oil, with its dynamic viscosity $\mu = 0.0087\text{Pa}\cdot\text{s}$ and working temperature 300 K. The inner diameter of the O-ring is $\phi 40 \pm 0.3$ mm, and the cross-sectional diameter is $\phi 1.8 \pm 0.08$ mm. The compression ratio of the O-ring reaches 26.11% after installation. After sealing, both the force inside the groove and

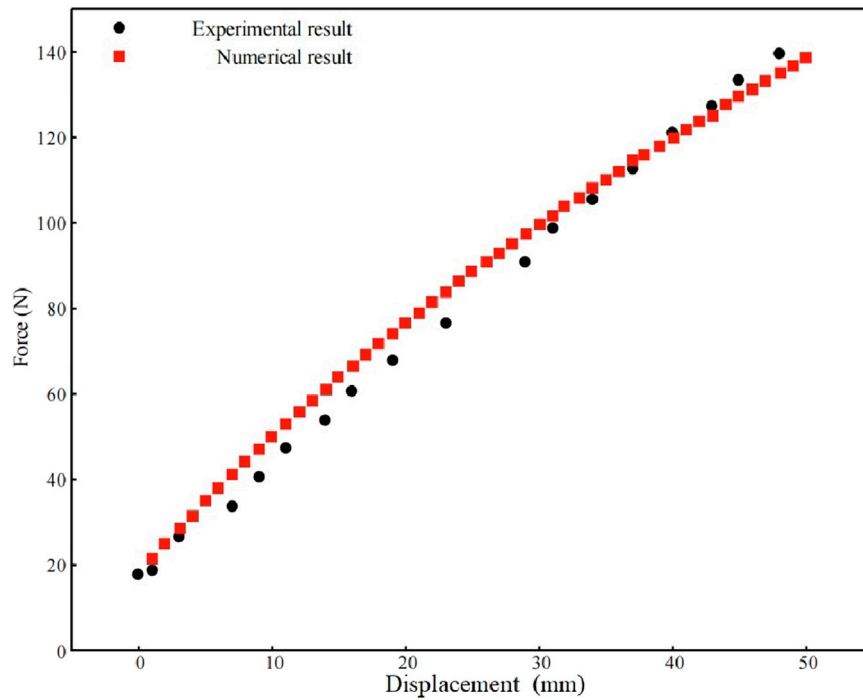


FIGURE 6 Comparison of simulation tension and test tension under the same tensile displacement.

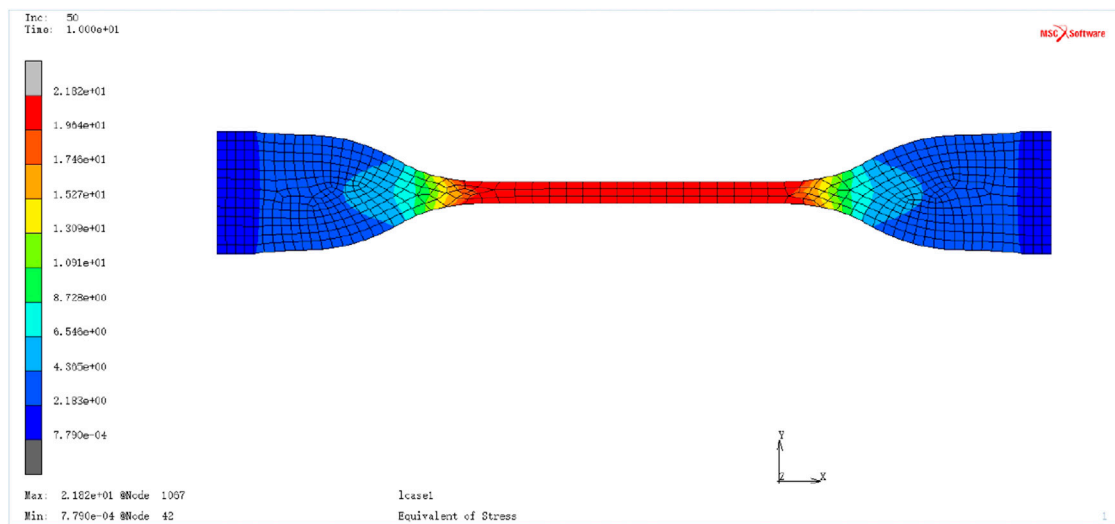


FIGURE 7 Simulation equivalent stress diagram of the specimen.

the internal medium pressure are axially symmetrically distributed. Therefore, the sealing part of the O-ring is simplified into a two-dimensional axisymmetric model.

Given the significant deformation of the O-ring, the nonlinear finite element software MSC. Marc was employed. To eliminate errors induced by unreasonable mesh sizes, three mesh seed spacing schemes were designed: the coarse mesh had an average element size of 0.04 mm with a total number of

elements of approximately 1,500; the medium mesh featured an average element size of 0.03 mm with around 2,800 total elements; and the fine mesh adopted an average element size of 0.02 mm with a total element count of roughly 6,300. The maximum contact pressure at the O-ring-metal interface was selected as the key verification index. When the mesh was refined from the coarse to the medium scheme, the relative variation in the maximum contact pressure reached 8.5%; whereas when

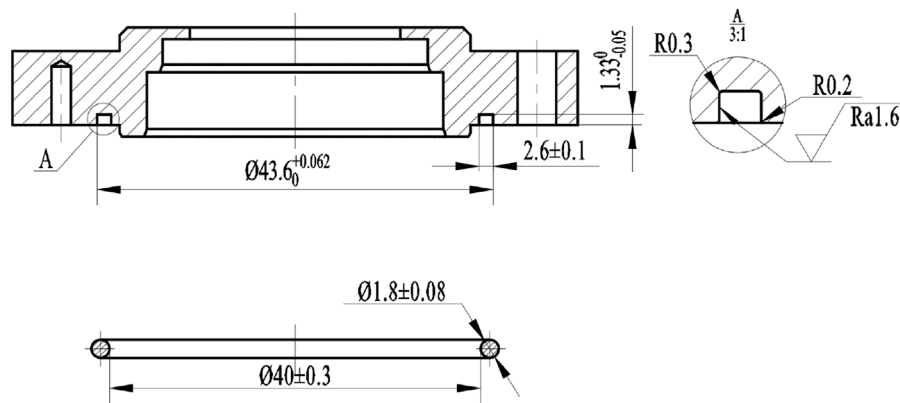


FIGURE 8
Dimensions and groove structure of O-ring.

further refined from the medium to the fine scheme, this relative variation decreased to less than 2.5%, indicating that the calculation results had tended to stabilize. Consequently, the medium mesh scheme was finally selected as the formal mesh for subsequent numerical simulations. For the nonlinear contact analysis involving hyperelasticity and large deformations, three core convergence criteria were implemented in MSC. Marc: force, displacement, and energy convergence. A single criterion is inadequate to address both rubber material nonlinearity and geometric nonlinearity, whereas the synergistic application of the three criteria guarantees the accuracy and robustness of simulation results.

The flange is assumed to be a rigid body, and the O-ring rubber seal is regarded as a deformable body. The boundary conditions are set so that the contact area between the workpiece and the O-ring does not bear pressure—ensuring the real pressure-bearing surface is only the unit edge where the O-ring deformable body and the rigid body do not contact. Meanwhile, according to the actual sealing pressure, the applied load is a surface force, with the pressure always acting perpendicularly on the unit boundary. The simulation model is shown in Figure 9.

4 Results

4.1 Contact pressure and contact length of the O-ring

During the initial compression process, the sealing groove remains stationary. As the upper cover plate slowly moves rightward, the O-ring undergoes compression deformation and makes contact with both the upper cover plate and the groove. The resilience generated by the deformation acts on the upper cover plate and the groove bottom surface, thereby generating initial compressive stress—i.e., the sealing pressure. The ratio of the O-ring's compression amount to its initial cross-sectional diameter is defined as the O-ring compression rate. As shown in Figure 10, there is nearly a linear relationship between the O-ring compression rate ε and the maximum sealing pressure p_{\max} . The

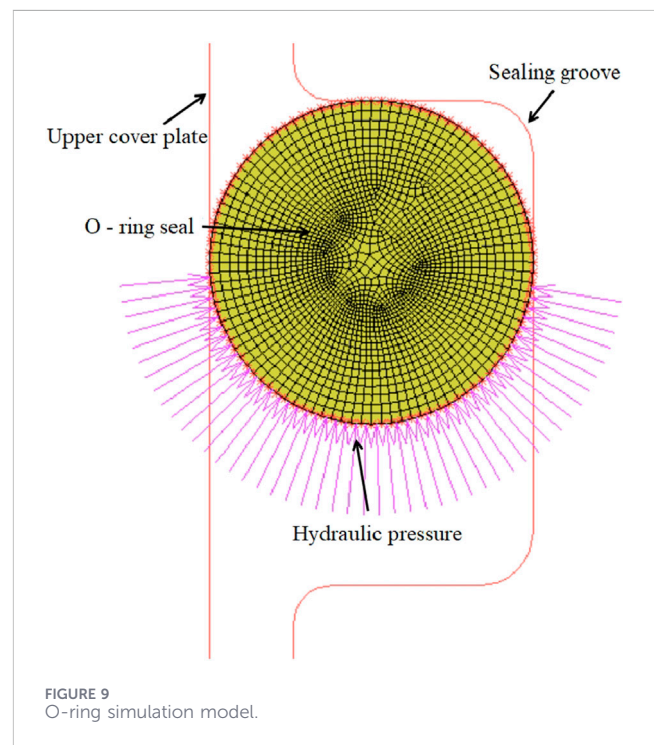


FIGURE 9
O-ring simulation model.

greater the compression rate, the higher the sealing pressure. However, a relatively high compression rate can cause the O-ring to experience permanent deformation, lose elasticity, and thereby fail in sealing.

In the working state, the simulation slowly applies liquid pressure differences of 0.3 MPa and 0.6 MPa to one side of the O-ring through the gap. At this point, the maximum sealing pressure p_{\max} increases to 1.216 MPa and 1.502 MPa respectively, and then remains unchanged, as shown in Figure 11. This is because during operation, the greater the liquid pressure difference on both sides of the O-ring seal, the greater the deformation of the O-ring, and the greater the pressure transmitted to the contact surface—thereby enhancing the sealing effect. This is termed the self-tightening sealing action.

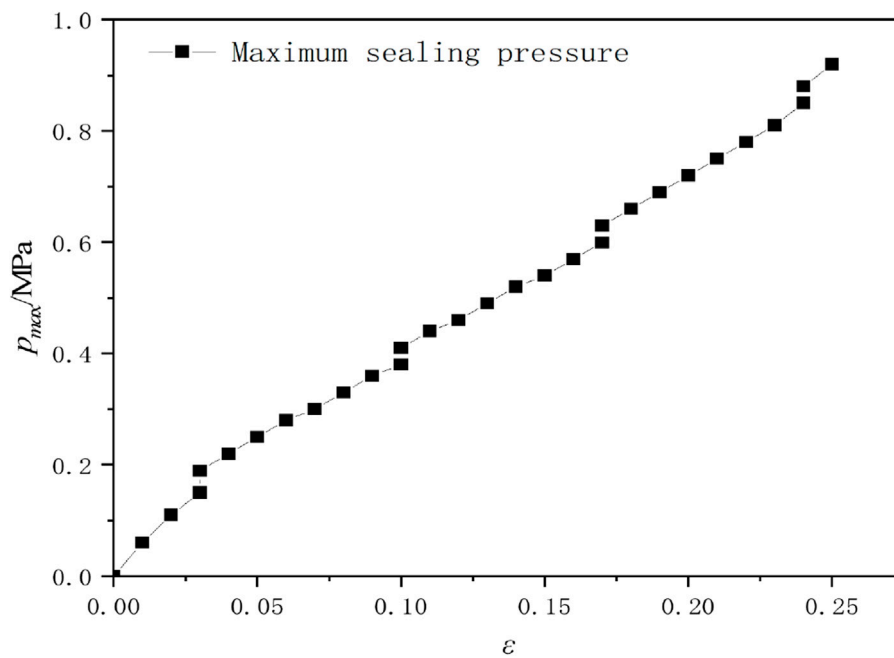


FIGURE 10 O-ring compression rate and maximum sealing pressure curve.

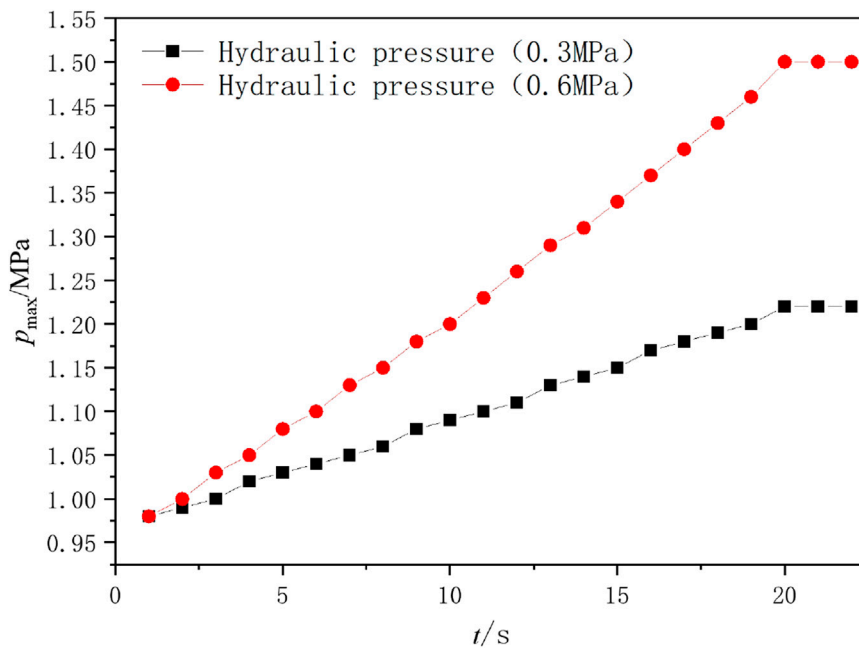
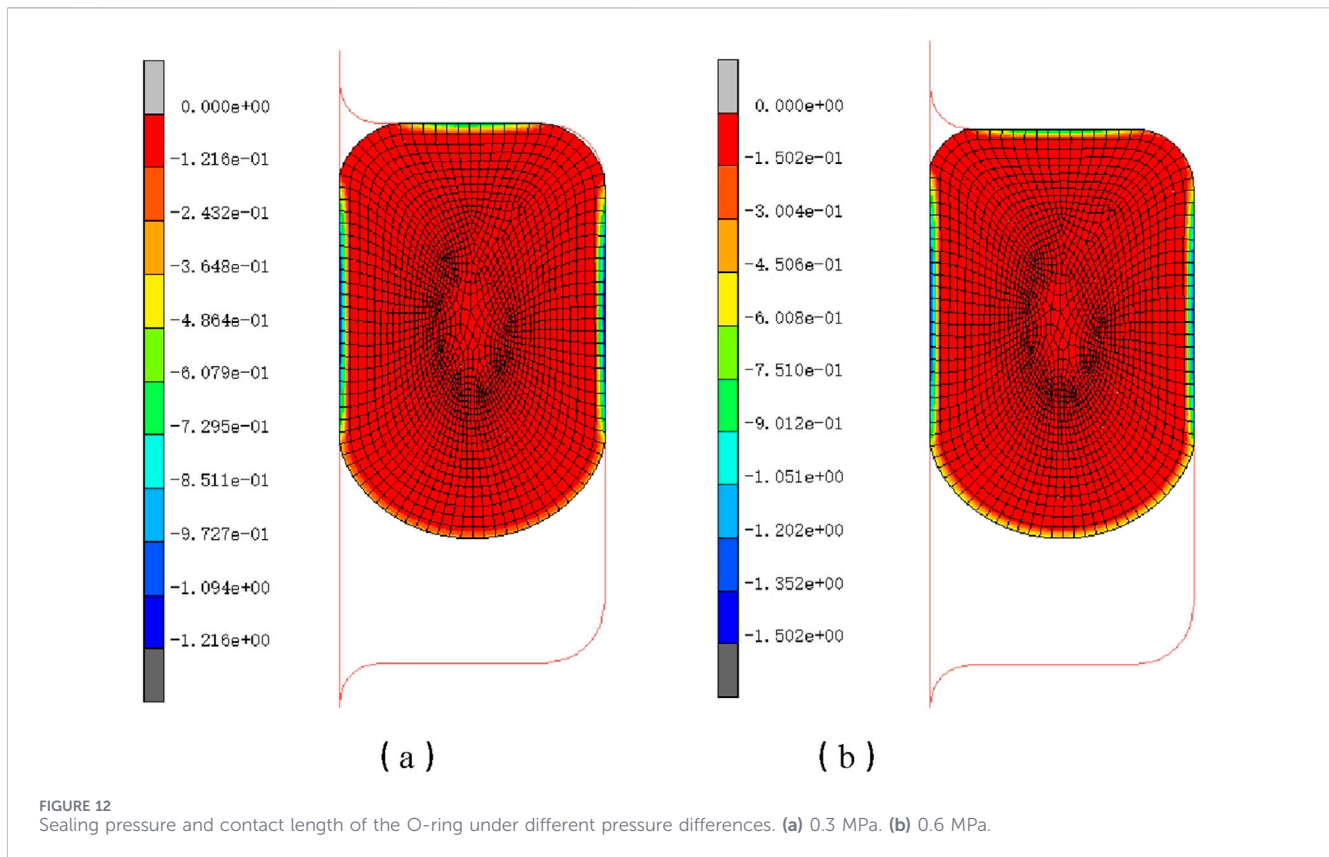


FIGURE 11 Curve of O-ring sealing pressure varying with liquid pressure.

The contact line between the O-ring and the groove is relatively long. Due to the self-tightening sealing effect, leakage often occurs between the O-ring and the upper cover plate. Therefore, in the calculation of leakage volume, the sealing contact length between the O-ring and the upper cover plate (referred to as “contact length” hereinafter) is the difference between the outer diameter and inner diameter at the sealing contact area. As shown in Figures 12a,b

respectively present the magnitude of sealing pressure at each position of the O-ring and the location of sealing contact length under internal and external liquid pressure differences of 0.3 MPa and 0.6 MPa.

As illustrated in Figure 13, along the contact length of the O-ring, the sealing pressure differs across distinct contact positions. The sealing pressure at both ends is relatively lower, whereas the pressure in the



middle is higher, exhibiting an arch-shaped distribution. When the sealed liquid pressure differences reach 0.3 MPa and 0.6 MPa, the sealing contact length w between the O-ring and the upper cover plate extends from 1.13 mm to 1.24 mm. The contact width varies under different pressure differences, and the outer contact radius r_2 of the seal satisfies the relationship: $r_2 = r_1 + w$ (where r_1 is the inner contact radius and w is the contact width). The inner side of the O-ring is in contact with the high-pressure medium, and its inward deformation is constrained by the medium pressure. Therefore, the inner contact radius of the seal remains basically stable under different pressure differences, which is consistent with the original inner radius. Based on the fitting of the sealing self-tightening effect law, a higher pressure difference results in a stronger extrusion force pushing the O-ring toward the sealing surface, and thus the contact length increases with the corresponding increase in pressure difference. Concurrently, the sealing pressure p at the contact area increases accordingly, with the maximum sealing pressure values under these two conditions differing by approximately 0.3 MPa.

4.2 Sealing clearance and correction factor

The number of annular micro-elements was set as $N = 20$. When $Ra = 0.8 \mu\text{m}$ (classified as a low-to-moderate roughness surface), $T = 1$ was adopted; when $Ra = 1.6 \mu\text{m}$ (classified as a moderate roughness surface), $T = 2 \mu\text{m}$ was adopted; and when $Ra = 3.2 \mu\text{m}$ (classified as a high roughness surface), $T = 3$ was adopted. The sealing clearance h (μm) and correction factor μ_1 were calculated by substituting the above simulation data into the formula, respectively. As illustrated in Figures 14, 15, the sealing clearance h and correction factor μ_1 of the O-ring seal

exhibit a consistent and physically interpretable trend with the variation of surface roughness and pressure difference (Δp): when Ra is fixed, both h and μ_1 decrease monotonically as Δp increases from 0.4 MPa to 1.6 MPa; conversely, when Δp is kept constant, larger Ra values lead to larger magnitudes of h and μ_1 . These trends are dominated by the coupling effect between pressure-driven elastic deformation and surface topography. Specifically, a higher Δp increases the contact pressure acting on the O-ring, prompting elastic deformation to fill the microscopic gaps on the sealing surface, thereby reducing the effective sealing clearance h and the proportion of active leakage channels. In contrast, a larger Ra results in more pronounced peak-valley uneven structures on the sealing surface, which form wider and more persistent microscopic gaps that cannot be completely eliminated by the elastic deformation of the O-ring. This consequently leads to an increase in h and a higher density of unclosed leakage channels.

4.3 Leakage rate

By substituting these parameters into Equation 7, the leakage rates Q corresponding to the three surface roughness levels ($Ra = 0.8 \mu\text{m}$, $Ra = 1.6 \mu\text{m}$, and $Ra = 3.2 \mu\text{m}$) under different sealing pressures Δp were obtained, as illustrated in Figure 16.

When the differential pressure Δp is relatively low, the leakage rate remains at a low level, yet as Δp increases, the leakage rate exhibits a near-linear upward trend across all roughness groups. For identical Δp , a greater surface roughness value consistently leads to a higher leakage rate: for example, at $\Delta p = 0.4 \text{ MPa}$, the leakage rate is $0.37 \times 10^{-12} \text{ m}^3/\text{s}$ for $Ra = 0.8 \mu\text{m}$, rising to $0.50 \times 10^{-12} \text{ m}^3/\text{s}$ for $Ra = 1.6 \mu\text{m}$ and $0.67 \times 10^{-12} \text{ m}^3/\text{s}$ for $Ra = 3.2 \mu\text{m}$. The underlying

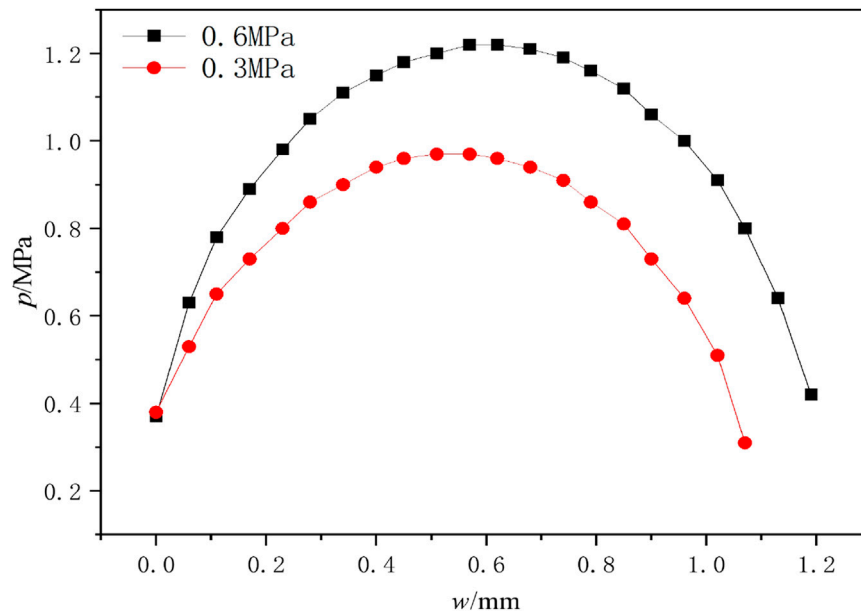


FIGURE 13 Sealing pressure curves at different positions along the contact length.

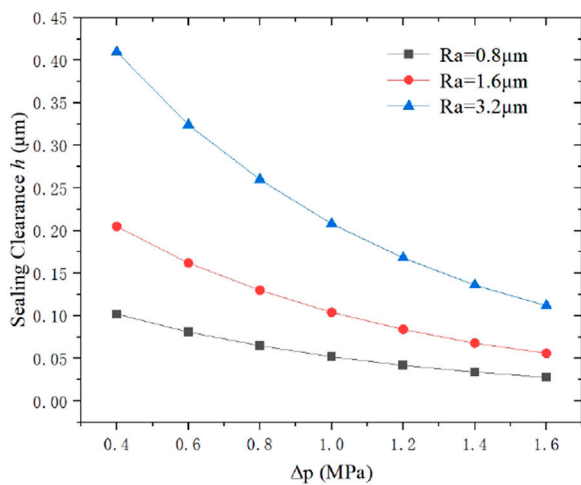


FIGURE 14 Sealing clearance h .

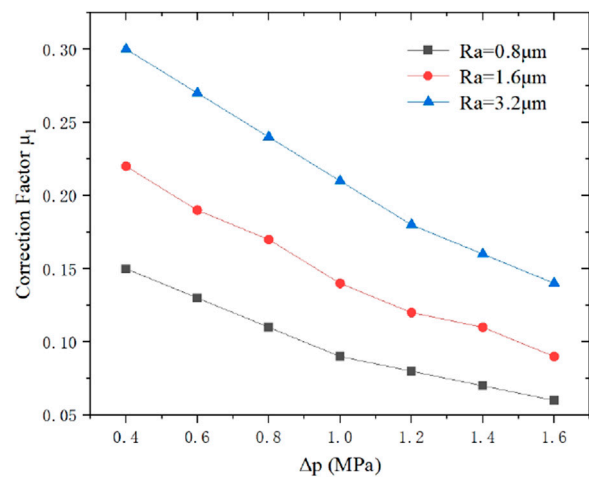


FIGURE 15 Correction factor μ_1 .

mechanism lies in two coupled effects: first, an increase in Δp elevates the pressure gradient driving fluid flow through micro-leakage channels, directly enhancing the leakage flux. Second, larger Ra values reflect more pronounced surface asperities, which create wider and more persistent leakage pathways that cannot be fully eliminated by the elastic deformation of the O-ring under contact pressure. Even as Δp increases and contact pressure rises to compress the sealing interface, the rough surface topography retains unclosed gaps, sustaining fluid flow. This observation aligns with the principle that surface roughness dominates the initial leakage channel formation, while differential pressure governs the subsequent flux through these channels.

5 Experimental verification and discussion

5.1 O-ring compression-rebound performance test

Before the test, the samples shall be placed at standard temperature for no less than 3 h. Subsequently, the cross-sectional diameter ϕ was measured, and the samples were installed into the test device according to the specified compression amount and duration for testing, with the compressed cross-sectional diameter ϕ_1 measured thereafter.

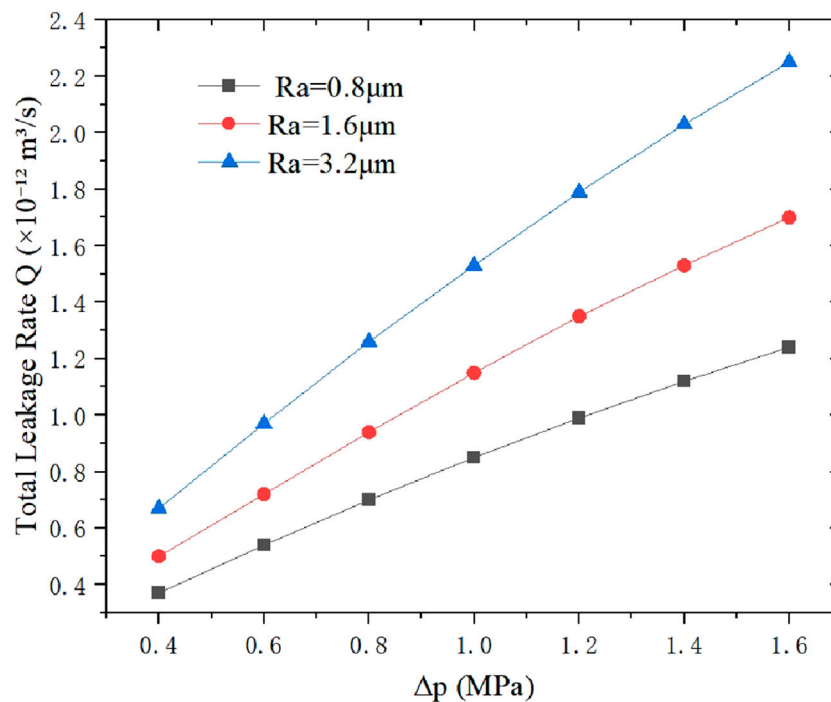


FIGURE 16
Total leakage rate curve under different liquid pressure difference.

After the test, the samples were removed from the test device, allowed to undergo natural recovery at standard temperature for 3 h, and then their recovered cross-sectional diameter ϕ_2 was measured. The test rig for the compression-rebound performance test is shown in Figure 17.

The compression rebound rate is calculated using Equation 14:

$$\varepsilon = (\phi_2 - \phi_1) / (\phi_0 - \phi_1) \times 100\% \quad (14)$$

Parameters in the formula: ε —Compression rebound rate (%); ϕ_0 —Original cross-sectional diameter of the sample before compression (mm);

ϕ_1 —Cross-sectional diameter of the sample after compression as specified (mm);

ϕ_2 —Effective cross-sectional diameter of the sample after recovery from compression (mm).

Based on the experimental data, as shown in Table 1, the compression rebound rates of the O-ring all fall within a reasonable range. In addition, the overall rebound rate is relatively high, with a minimum value of 97.83%, and most values are close to or reach 100%, indicating that the O-ring exhibits excellent rebound recovery performance after compression.

5.2 Leakage volume measurement experiment and discussion

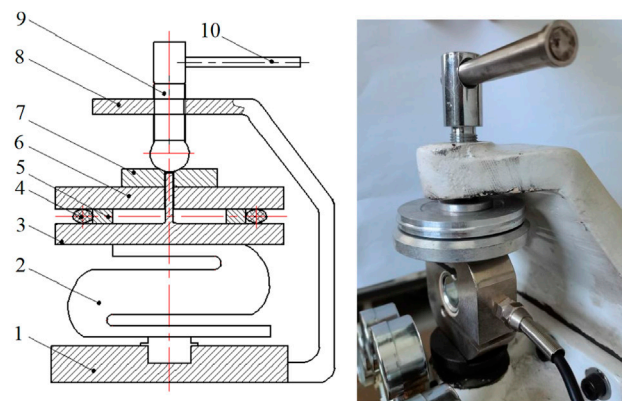
The static sealing structure system mainly consists of a grooved flange, a baffle plate, an oil collecting cup, and a precision pressure regulation system. The hydraulic system comprises a pressure transmitter, a relief valve, and oil circuit connecting pipes. The

collection system includes an oil pan for capturing leaked oil, oil pipes for guiding fluid flow, and a dry beaker for collecting the leaked oil. A constant room temperature was maintained throughout the experiments to avoid the influence of oil temperature fluctuations on oil viscosity, and no additional vibration was applied to the sealing system. The test rig is capable of providing adjustable pressures ranging from 0 to 2.0 MPa to the sealing test cavity, thereby establishing the required operating conditions for O-ring sealing tests. The experimental test rig and experimental flow chart are depicted in Figure 18.

This study experimentally investigates the leakage characteristics of O-ring seals under differential pressures of 0.3 MPa and 0.6 MPa, with surface roughness values of 0.8 μm , 1.6 μm and 3.2 μm .

The metal sealing surface in contact with the O-ring adopts 316L austenitic stainless steel as the base material, as shown in the top-left corner of Figure 18. A flat basic surface is first obtained via CNC turning, followed by grinding with grinding wheels of different grit sizes to control the surface roughness: grinding with an 80-grit coarse grinding wheel yields a surface with a roughness $Ra = 3.2\mu\text{m}$; replacing it with a 120-grit medium grinding wheel produces a surface with $Ra = 1.6\mu\text{m}$; fine grinding with grinding wheels of 240 grit or finer, coupled with polishing using a polishing cloth, enables the preparation of a surface with $Ra = 0.8\mu\text{m}$.

To determine the Ra parameter, a surface roughness tester was used to select at least 3 different measurement points along the circumferential and radial directions of the sealing surface. The Ra value at each measurement point was recorded and the average value was calculated, so as to ensure the reliability of the measured data.



1.Base 2.Pressure Sensor 3.Lower Pressure Plate 4.O-Ring 5.Restriction Ring 6.Upper Pressure Plate 7.Top Plate 8.Support Plate 9.Spiral Clamping Rod 10.Extended Handle

FIGURE 17
Compression-rebound performance test rig.

TABLE 1 Calculation table of compression rebound rate.

Parameter	Sample 1	Sample 2	Sample 3	Sample 4
Total thickness of the upper and lower pressure plates	17.65	17.60	17.63	17.62
Total thickness of the upper and lower pressure plates and the O-ring after compression	18.99	18.91	18.96	18.94
ϕ_0	1.34	1.31	1.33	1.32
ϕ_1	1.80	1.81	1.80	1.80
ϕ_2	1.80	1.80	1.79	1.80
ε	100%	98%	97.83%	100%

The cumulative leakage volume is measured over a 24-h period using a gravimetric method, where the leaked hydraulic oil is collected via an oil pan, oil pipe and dry beaker with a hydraulic oil density of 0.85 mg/ μ L. The theoretical cumulative leakage volumes and experimental cumulative leakage volumes under the differential pressures of 0.3 MPa and 0.6 MPa are denoted as Q_{V1} , Q_{V2} , Q_{V3} and Q_{V4} , respectively. As shown in Figure 19, the theoretical cumulative leakage volume of the O-ring seals ranges from 33.60 μ L to 85.44 μ L under the test conditions. The relative error between experimental and theoretical values is controlled within 15% with random deviation directions. Specifically, a higher experimental leakage volume than the theoretical value is observed in the case of 0.3 MPa differential pressure and 0.8 μ m surface roughness, which is attributed to micro-burrs on the sealing surface that widen the local leakage channels beyond the scope of theoretical assumptions. In contrast, a lower experimental value appears under 0.3 MPa differential pressure and 1.6 μ m surface roughness, resulting from the elastic rebound of the O-ring material after long-term compression, which reduces the actual sealing gap. For the condition of 0.6 MPa differential pressure and 1.6 μ m surface roughness, the experimental leakage volume exceeds the theoretical value due to the random distribution of micro-leakage paths on the rough sealing surface that cannot be fully characterized by the idealized theoretical

model. Meanwhile, the experimental value is lower than the theoretical value under 0.6 MPa differential pressure and 3.2 μ m surface roughness because of slight oil adhesion on the inner wall of the oil pipe during the collection process. The remaining test cases show a relative error below 10%. These results demonstrate that the experimental data meet the precision requirements of mechanical seal tests, validating the accuracy of the circular plate micro-element integral model for O-ring leakage prediction. This confirms that the overall uncertainties of the proposed model are controllable under specific conditions, i.e., room temperature, low pressure and short-term service.

Meanwhile, the random deviations between experimental and theoretical values are closely related to the micro-topography of the sealing surface, elastic deformation of the O-ring material, and oil adhesion during the measurement process, rather than temperature-related factors.

6 Conclusion

This study proposed an optimized leakage prediction model for O-ring static seals based on the circular-plate gap theory, in which a novel leakage rate correction factor was incorporated to quantify the effect of surface roughness on micro leakage channels. The numerical

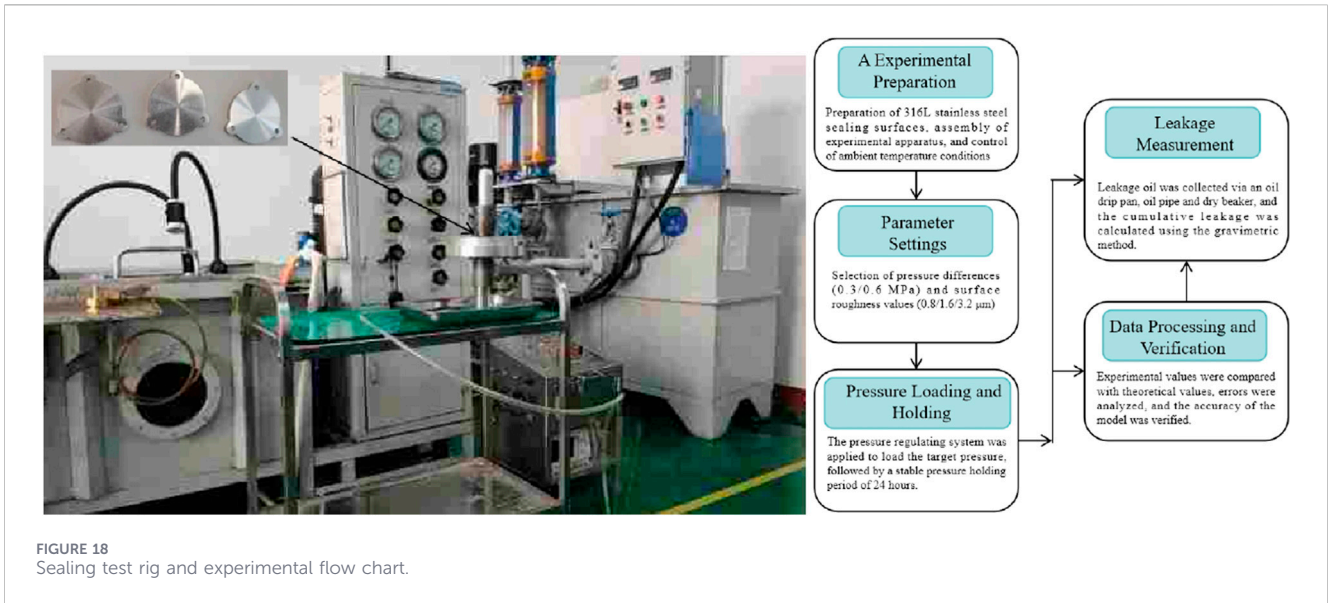


FIGURE 18 Sealing test rig and experimental flow chart.

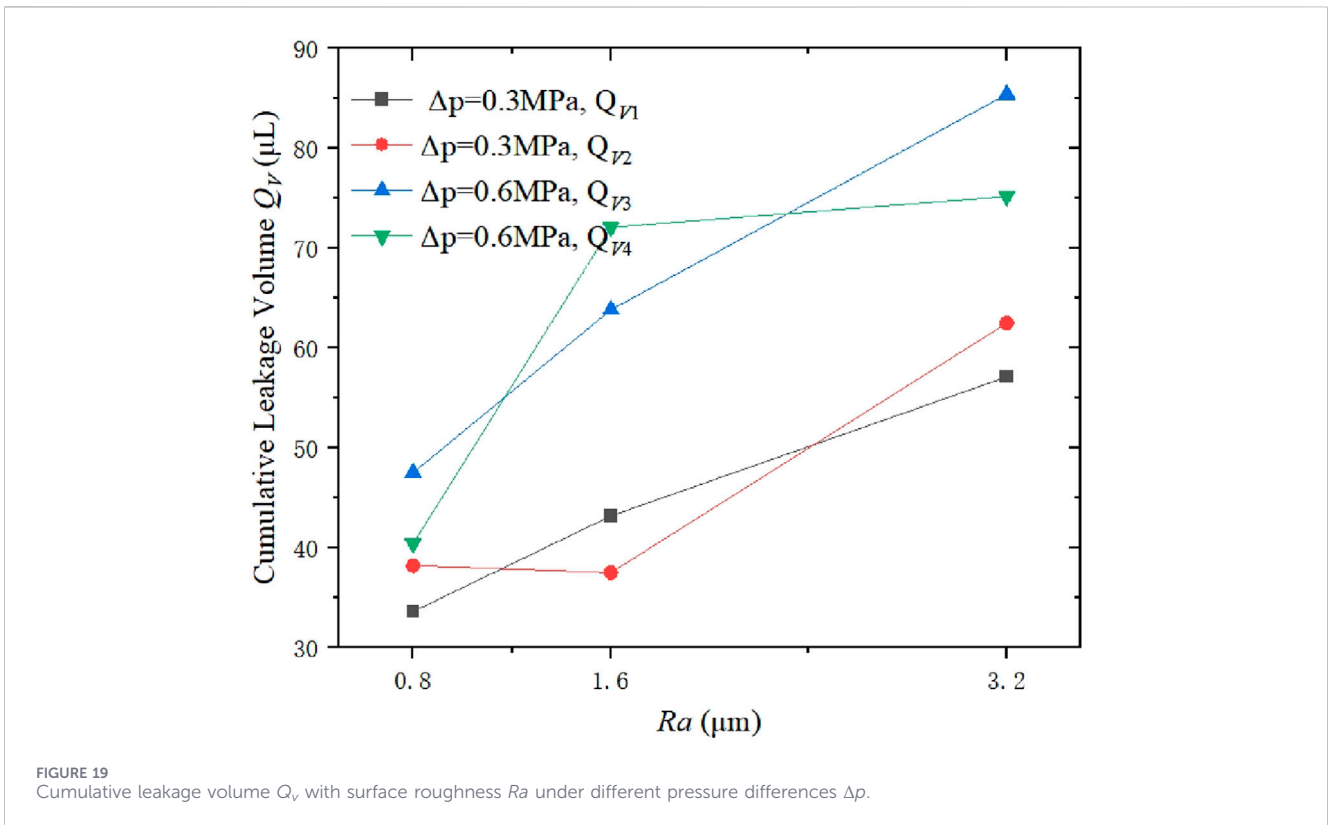


FIGURE 19 Cumulative leakage volume Q_v with surface roughness Ra under different pressure differences Δp .

and experimental results showed that under the differential pressure range of 0.3–0.6 MPa, the contact pressure along the sealing interface exhibited an obvious arch-shaped distribution, and the effective contact length increased quantitatively from 1.13 mm to 1.24 mm with the increase of pressure difference. The leakage rate increased with the increase of differential pressure and surface roughness Ra , and the leakage rate at $Ra = 3.2 \mu\text{m}$ was approximately 1.8 times that at $Ra = 0.8 \mu\text{m}$ under the same working pressure, which revealed the

quantitative coupling mechanism of roughness and pressure on leakage characteristics. In the experimental validation, the 24-h cumulative leakage volume varied from 33.60 μL to 85.44 μL , and the relative error between the predicted and measured values was controlled within 15%, with most working conditions below 10%, indicating strong prediction consistency. Under room temperature, low pressure and short-term service conditions, the sealing interface remained stable, and the model could accurately reflect the leakage

variation mechanism caused by pressure load and surface topography. Although the surface roughness was simplified into regular conical peaks and the effects of high temperature, long-term aging and extreme high pressure were not considered, the proposed leakage model still showed favorable stability and accuracy in engineering leakage prediction for conventional working conditions. In summary, the circular-plate gap leakage model established in this study provided an effective quantitative method for O-ring seal design and leakage evaluation. However, this model is currently limited to room-temperature, low-pressure and short-term applications, and the extension to more complex service environments remains an important direction to be explored in future research.

Data availability statement

The original contributions presented in the study are included in the article/supplementary material, further inquiries can be directed to the corresponding author.

Author contributions

ZW: Writing – original draft, Writing – review and editing. G-hZ: Methodology, Writing – review and editing, Investigation, Data curation, Formal Analysis, Software.

Funding

The author(s) declared that financial support was received for this work and/or its publication. This study was supported by Henan

Province Science and Technology Research Project (No. 242102220065). The authors gratefully acknowledge this financial support.

Conflict of interest

Author(s) G-hZ was employed by Shanghai Microelectronics Equipment (Group) Co., Ltd.

The remaining author(s) declared that this work was conducted in the absence of any commercial or financial relationships that could be construed as a potential conflict of interest.

Generative AI statement

The author(s) declared that generative AI was not used in the creation of this manuscript.

Any alternative text (alt text) provided alongside figures in this article has been generated by Frontiers with the support of artificial intelligence and reasonable efforts have been made to ensure accuracy, including review by the authors wherever possible. If you identify any issues, please contact us.

Publisher's note

All claims expressed in this article are solely those of the authors and do not necessarily represent those of their affiliated organizations, or those of the publisher, the editors and the reviewers. Any product that may be evaluated in this article, or claim that may be made by its manufacturer, is not guaranteed or endorsed by the publisher.

References

- Huon, C., Tiwari, A., Rotella, C., Mangiagalli, P., and Persson, B. N. J. (2021). Air, helium and water leakage in rubber O-ring seals with application to syringes. *Tribol. Lett.* 70, 35. doi:10.1007/s11249-022-01574-7
- Kerr, T., and Nielson, J. (2022). Dynamic seal test rig: O-ring leakage and sliding friction measurements. Volume 8A: structures and dynamics—aerodynamics excitation and damping; bearing and seal dynamics; emerging methods in engineering design, analysis, and additive manufacturing; fatigue, fracture, and life prediction. doi:10.1115/gt2022-82221
- Mo, L., Xiao, X., Chen, Y., Fang, M., Xiao, S., Yong, H., et al. (2025). A rapid decompression failure mechanism model coupling diffusion-deformation of O-ring sealing rubber exposed to high-pressure carbon dioxide. *Eng. Fail. Anal.* 170, 109271. doi:10.1016/j.engfailanal.2025.109271
- Persson, B. N. J. (2022). Fluid leakage in static rubber seals. *Tribol. Lett.* 70 (2), 1–10. doi:10.1007/s11249-022-01573-8
- Qi, Z., Ma, R., and Li, S. (2023). Sealing performance and deformation failure analysis of high pressure flange metal O-ring with open holes. *Huagong Jinzhan/Chem. Industry Eng. Prog.* 42, 166–174.
- Roth, A. (1972). The interface-contact vacuum sealing processes. *J. Vac. Sci. Technol.* 9 (1), 14–23. doi:10.1116/1.1316537
- Song, Y., Yu, B., and Hao, M. (2024). Dynamic tracking performance analysis of liquid-film seal based on thermal-fluid-structure coupling. *Zhendong yu Chongji/J. Vib. Shock* 43 (7), 214–222.
- Tong, G., Zhu, X., Liu, Y., Lv, F., and Lu, X. (2024). Research on the sealing mechanism of split-liner high-pressure hydrogen storage cylinders. *Processes* 12 (3), 16. doi:10.3390/pr12030554
- Vijayaragavan, B., Asok, S. P., and Marichelvam, M. K. (2025). Optimizing the labyrinth geometric parameters and modelling a new twin seal configuration for improved sealing efficiency in gas turbines. *Front. Mech. Eng.* 11, 1440903. doi:10.3389/fmech.2025.1440903
- Wang, Q., Liu, D., and Liu, Z. (2023). A leakage rate calculation method for O-ring seal based on compound leakage channel model. *J. Mech. Eng.* 59 (11), 232–241.
- Wu, J. B., Li, L., and Wang, P. J. (2024). Effect of stress relaxation on the sealing performance of O-rings in deep-sea hydraulic systems: a numerical investigation. *Eng. Sci. Technol. Int. J.* 51, 101654. doi:10.1016/j.jestch.2024.101654
- Wu, J. B., Li, L., and Wang, P. J. (2024). Study on the effects of three surface imperfections on the performance of O-ring seals based on the finite element method. *Proc. Institution Mech. Eng. Part C. J. Mech. Eng. Sci.* 238 (20), 10158–10171. doi:10.1177/09544062241258911
- Yang, W. (2016). *Numerical analysis and theoretical Prediction Method of interface leakage characteristics in Hard sealing structure*. Wuhan, China: Huazhong University of Science and Technology.
- Yang, M., Xia, Y. M., Ren, Y., Zhang, B. w., and Wang, Y. (2023). Design of O-ring with skeleton seal of cutter changing robot storage tank gate for large diameter shield machine. *Tribol. Int.* 185, 108591. doi:10.1016/j.triboint.2023.108591
- Yasuo, Y., Ryutaro, T., and Tadanori, S. (2017). A new quantitative evaluation for characteristic of surface roughness in turning. *Precis. Eng.* doi:10.1016/j.precisioneng.2017.04.009
- Yu, Y., Gong, L., Wu, Y., He, G., Shi, Y., and Liu, X. (2025). Enhanced leakage prediction in lubricating-oil static seals considering surface texture orientation. *Tribol. Int.* 214, 10. doi:10.1016/j.triboint.2025.111160
- Zhang, J., and Xie, J. (2018). Investigation of static and dynamic seal performances of a rubber O-ring. *J. Tribol.* 140, 042202. doi:10.1115/1.4038959
- Zhao, Y., Feng, Z., and Yunchao, L. I. (2022). Analysis of contact surface wear performance of O-ring dynamic seal based on archard model. *Tech. Gaz./Teh. Vjesn.* 29 (5). doi:10.17559/TV-20210913080305
- Zhao, X., Liu, Y., and Guo, F. (2025). A quantitative characterization model for nonlinear dynamic parameters of O-rings. *Mech. Syst. Signal Process.* 224, 224. doi:10.1016/j.ymsp.2024.112176

Glossary

Q	the Leakage Rate
Q_V	Cumulative Leakage Volume
Ra	Surface Roughness
b	Width
u	the Liquid Flowing
μ	Dynamic Viscosity of the Fluid
μ_1	Leakage Rate Correction Factor
h	Sealing Clearance
Δp	Pressure Difference
N	the Number of Annular Micro-elements
r_1	the Inner Diameter of the Ring at the Sealing Contact
r_2	the Outer Diameter of the Ring at the Sealing Contact
δ	the Root Mean Square Deviation of the Surface Profile
T	the Surface Autocorrelation Length
λ	the Sealing Coefficient
I	Numerical Calculation Result of the Integral Term Within the Radial Sealing Range
W	the Strain Energy Density Function
w	the Contact Length
$C_{10} \setminus C_{01}$	Mooney-Rivlin Constants
ε	Compression Rebound Rate
ϕ_0	Original Cross-sectional Diameter of the Sample Before Compression
ϕ_1	Cross-sectional Diameter of the Sample after Compression as Specified
ϕ_2	Effective Cross-sectional Diameter of the Sample after Recovery from Compression